Second-law and life-cycle assessment of CO_2/R-1270 zeotropic blends in transcritical vapour-compression cycles under summer Arabian Gulf conditions

Abdulaziz Alsahali

Dhahran Ahliyya Schools, Dhahran, Saudi Arabia. E-mail: alsahaliabdulaziz@gmail.com

Abstract

At high ambient temperatures, transcritical carbon dioxide loses COP rapidly. Zeotropic blends, which may offer a helpful solution for sustainable cooling while maintaining efficiency, have been studied largely in temperate climates with 25 to 35 °C, while there is an absence of studies under harsh Gulf summer climate conditions. The method used in this investigation was modelling the performance of carbon dioxide/R-1270 at zero to 15% R-1270 from 40 to 48 °C. The model uses a published pressure-ratio-dependent isentropic efficiency correlation, along with energy, exergy, and TEWI analysis. The blend lowered COP at every composition and ambient temperature, by −5.2% at 15% R-1270 and 40 °C. At 15% R-1270, the mixture's critical temperature increases by 6.2 K, against the 14 K required to bring the gas cooler outlet below the critical temperature. The internal heat exchanger (IHX) helped recover COP, with recovery increasing as ambient temperatures increased, from +7.7% at 40 °C to +13.0% at 48 °C. A takeaway from this investigation is that effort on improving internal heat exchange and expansion recovery systems in refrigeration may offer benefits over zeotropic blends in harsh Gulf climates.

Highlights

- R-1270 blending lowers transcritical CO_2 COP at all Gulf-summer conditions
- 15% R-1270 raises mixture T_{crit} by 6.2 K; 14 K needed to leave transcritical regime
- Blend COP penalty shrinks with ambient, −5.2% at 40 °C to −4.0% at 48 °C
- IHX recovers 7.7–13.0% COP but never offsets the blend penalty
- Compressor and valve destroy ~60% of exergy; prioritize IHX and expansion recovery

Keywords

internal heat exchanger; zeotropic mixture; transcritical carbon dioxide; exergy analysis; high ambient temperature

1. Introduction

Transcritical CO_2 is a leading natural-refrigerant option, as it excels in multiple factors. Its GWP is 1, and it is non-flammable while having zero ODP. However, its COP decreases rapidly at higher ambient temperatures because heat rejection happens at a higher temperature, which leads to the fluid entering the valve having a higher enthalpy and the loss due to throttling growing. The COP falls quickly with an increase in ambient temperature [1,2]. This penalty is most severe in warm and hot climates, where single-stage CO_2 systems lose efficiency unless the cycle is modified [3–5]. In the Arabian Gulf, daytime summer temperatures of 40–48 °C coincide with the peak of air-conditioning demand [4,5].

Several approaches to the problem have been studied: internal heat exchange, ejectors, parallel compression, mechanical subcooling and zeotropic blends [6–13]. The internal heat exchanger (IHX) recovers COP by exchanging heat between the gas-cooler outlet and the evaporator outlet, so that the stream entering the expansion valve is subcooled; experiments have confirmed this gain in transcritical CO_2 plants [10,14,15] and its value in warm climates [16]. Ejectors are a solution in which high-pressure gas from the gas cooler outlet is used to entrain low-pressure gas out of the evaporator, theoretically decreasing the work required for the same job [11]. Parallel compression bypasses the main compressor by rerouting flash gas from an intermediate-pressure receiver to a dedicated parallel compressor, which uses a high suction pressure that may save energy in warm climates [12,13]. Lastly, mechanical subcooling uses a secondary refrigeration system to cool the refrigerant leaving the gas cooler before it reaches the expansion valve [8].

A second route modifies the working fluid rather than the cycle. Zeotropic blends are composed of multiple refrigerants, so that they condense and change phase over a range of temperatures. Adding a less volatile component to CO_2 offers three potential benefits: the mixture critical temperature rises, so that heat rejection may approach or fall below the critical point; the optimal high-side pressure falls; and the temperature glide during phase change can be matched to the temperature profile of a secondary fluid, which reduces heat-transfer irreversibility.

Theoretical and laboratory studies have explored these benefits for several CO_2 blends. Kim et al. [9] showed that CO_2/propane mixtures improve cooling performance when the glide is matched to the secondary heat-transfer fluid. Dai et al. [17] evaluated blends of CO_2 with ten low-GWP fluids in a heat pump water heater and found that good thermal matching in the heat exchangers raised the COP, while the blends lowered the high-side pressure relative to pure CO_2. Yu et al. [18] reported performance improvements with a CO_2/propane mixture in automobile air conditioning, and Yelishala et al. [19,20] attributed the gains of hydrocarbon/CO_2 blends to temperature-glide matching in the heat exchangers. Dai et al. [8] placed a zeotropic mixture in the mechanical-

subcooling loop of a transcritical CO_2 cycle rather than in the main circuit. In all of these studies, the benefit relies on matching the glide to a secondary fluid.

For CO_2/R-1270 specifically, a series of experimental studies has been published. Sánchez et al. [6] selected CO_2/R-1270 and CO_2/R-32 blends that are theoretically non-flammable with a GWP below 150 and, in a vertical display cooler, measured energy-consumption reductions of up to 17.2% at 25 °C ambient and 12.2% at 30 °C relative to pure CO_2. Sánchez et al. [7] then tested CO_2/R-32, CO_2/R-1234yf and CO_2/R-1270 in a transcritical refrigerating plant with and without an IHX, and developed an empirical model of a semihermetic reciprocating compressor operating with different CO_2-based mixtures [21]. Vidan-Falomir et al. [22] tested CO_2/R-1270 at 97/3, 94/6 and 91/9 by mass over heat-rejection temperatures of 20–34 °C and reported COP improvements of up to 12.2%, with the heat-rejection pressure reduced by 14.9 bar at 34 °C. Larrondo-Sancho et al. [23] tested 4% and 6% R-1270 and R-290 in a single-stage plant with an IHX at heat-rejection temperatures of 20, 27 and 34 °C; COP improved by up to 9.7% with 4% R-1270, and compressor power fell by 1.2–7.4%, which the authors attributed mainly to improved compressor efficiency with the mixtures. Table 3 summarises these studies. All of these gains were measured at heat-rejection temperatures of 34 °C or below.

The vast majority of studies regarding zeotropic blends are fitted for temperate environments with European ambient temperatures of 25–35 °C, while few have tested the benefits and trade-offs at higher ambient temperatures consistent with Gulf summer climates. No study has evaluated CO_2/R-1270 at 40–48 °C ambient, where the gas-cooler outlet (45–53 °C) lies well above the mixture critical temperature, and none combines energy, exergy and TEWI analysis for this blend. This paper simulates CO_2/R-1270 zeotropic blends from 0–15% R-1270 across a range of temperatures (40–48 °C) and analyses energy, exergy and TEWI, to determine whether the blend still raises the COP under Gulf summer conditions and, if not, why. In summary, the blend does not confer any benefit, and the reason for that is the gap in critical temperature, which is 6.2 K gained against 14 K needed to reach the gas cooler outlet.

2. Methods

2.1 Cycle configuration

A vapour-compression cycle was modelled in which the refrigerant passes through six different state points. There are two different versions of the cycle, one with an internal heat exchanger (IHX) and one without. The working fluid is transcritical CO_2, chosen for its GWP of 1, non-toxicity, non-flammability, and zero ODP. A zeotropic blend of CO_2 and R-1270 was also modelled, with the aim of recouping efficiency losses due to CO_2 being in a transcritical state. The

IHX allows for heat exchange between the high-pressure and low-pressure streams. Fig. 1 shows the layout and Fig. 2 the corresponding T–s diagram. The six state points the refrigerant passes through are:

State 1: evaporator outlet / IHX cold-stream inlet
State 1b: IHX cold-stream outlet / compressor inlet
State 2: compressor outlet / gas cooler inlet
State 3: gas cooler outlet / IHX hot-stream inlet
State 3b: IHX hot-stream outlet / expansion valve inlet
State 4: expansion valve outlet / evaporator inlet
Without the IHX, states 1 and 1b, and 3 and 3b, coincide.

Heat absorbed at the evaporator is rejected at the gas cooler. Heat is also exchanged internally from the high-pressure stream to the suction stream. The coefficient of performance (COP) is

(1)

where h denotes specific enthalpy. When the IHX is active, the gas-cooler outlet (hot stream) is cooled by the evaporator outlet (cold stream) through heat exchange, thereby increasing the refrigerating effect.

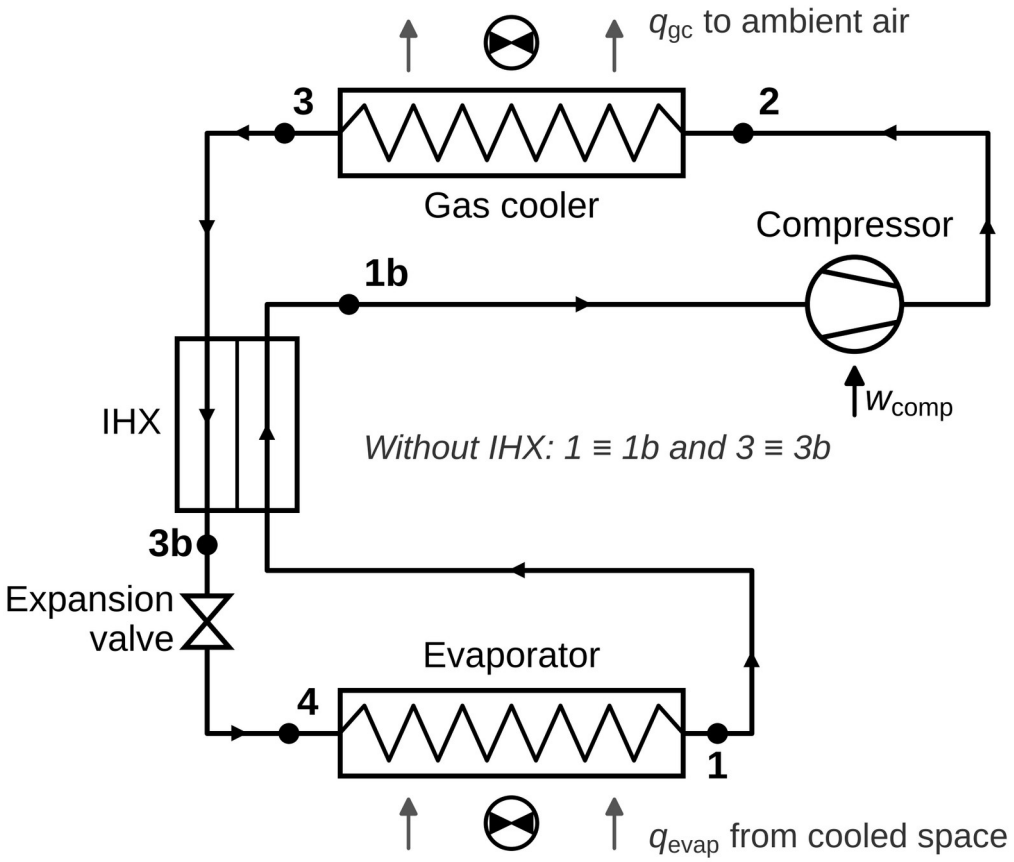


Fig. 1. Process scheme of the transcritical CO_2/R-1270 cycle with internal heat exchanger (IHX), drawn with conventional engineering symbols (ISO 10628-2): compressor, air-cooled gas cooler and evaporator with fans, counter-flow IHX and expansion valve. High-pressure side: states 2, 3 and 3b; low-pressure side: states 4, 1 and 1b. Without the IHX, states 1 ≡ 1b and 3 ≡ 3b.

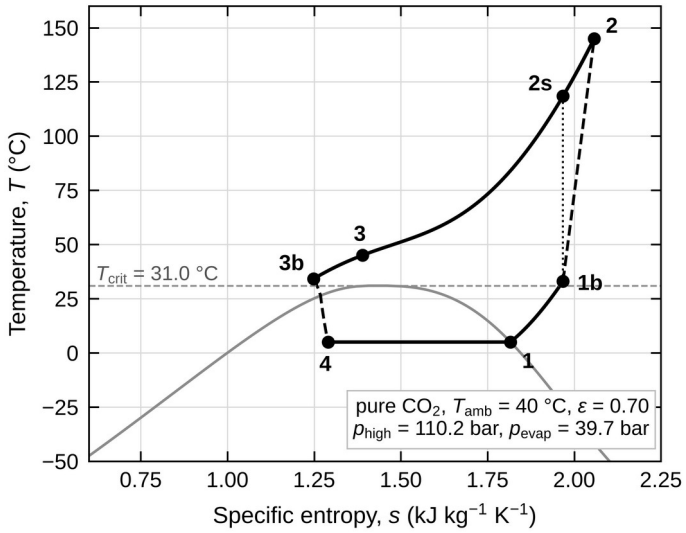


Fig. 2. Temperature–entropy diagram of the IHX cycle for pure CO_2 at T_{amb} = 40 °C and ε = 0.70, computed with the present model. State 2s is the isentropic discharge state; dashed lines show the irreversible compression (1b–2) and throttling (3b–4); the grey dashed horizontal line marks the CO_2 critical temperature.

2.2 Thermodynamic properties

All substances, including pure and mixture substances, were evaluated in CoolProp 8.0.0 [24] through a Helmholtz-energy backend (HEOS). Mixture compositions are specified as R-1270 mass fractions. Pure CO_2 was described by the equation of state of Span and Wagner (1996) [25]. Pure R-1270 was described by the equation of state of Lemmon et al. [26,27]. The binary mixture was described by a multi-fluid Helmholtz model [28], with reducing parameters of R-1270 and CO_2 fitted by Bell and Lemmon (2016) [29] (β_T = 0.98798, γ_T = 0.93465, β_V = γ_V = 1, as published). Excess Helmholtz contributions beyond the reducing-parameter fit are neglected. This is a recognized limitation of the method.

2.3 Operating conditions and assumptions

The evaporating (dew-point) temperature was set to 5 °C. This was done to cater to the application of the cycle, which is space cooling. The gas-cooler outlet temperature is the ambient temperature increased by 5 K, which is justified by limited gas cooler area and by air-cooled gas coolers operating slightly above ambient in real conditions. The baseline effectiveness of the internal heat exchanger is 0.70, which is a representative value of the 0–0.9 range swept in increments of 0.1 (see Section 2.8). In the exergy analysis, the dead-state pressure is 1.013 bar. The high-side pressure search window is 78–165 bar. All parameters are listed in Table 1.

Operating assumptions:

• Helmholtz contributions beyond the reducing parameters of Bell and Lemmon (2016) were not accounted for. This was because the departure function for the R-1270 and CO_2 pair is absent from CoolProp's database. This limits the accuracy of the blend and resulting calculations.

• Heat transfer to the surroundings was neglected in the adiabatic compressor and valve (states $1b \rightarrow 2$ and $3b \rightarrow 4$, respectively). This was because casing heat loss is small compared with the work input, and because the valve has negligible surface area and residence time.

• Chemical exergy was neglected throughout the cycle. The refrigerant's composition stays constant throughout and no reaction occurs, so every component carries the same chemical exergy and the term cancels.

• Steady-state operation; no pressure drop in any component or line; fixed circulating composition (no fractionation).

2.4 Compressor model

The compressor's isentropic efficiency is obtained from Okasha and Müller's performance data for a commercial semi-hermetic CO_2 compressor [30] as a cubic polynomial in pressure ratio:

(2)

with $b_0 = 0.7191$, $b_1 = -0.1358$, $b_2 = 0.0455$ and $b_3 = -0.0048$, as published [30]. The 0 °C row was used because its fitted pressure-ratio range (2.15–4.02) covers the present pressure ratios with and without the IHX (no IHX: 2.94–4.01; IHX: 2.78–3.73). The resulting isentropic efficiency is 0.59–0.60. Compression is modelled as adiabatic, so the discharge enthalpy follows from

(3)

where h_{2s} is the enthalpy at the discharge pressure and the suction entropy. Because no shell heat loss is modelled, the computed discharge temperatures (144–175 °C with the IHX) are an upper bound on those of a real machine.

2.5 High-side pressure optimization

As pressure increases, throttling loss reduces but the work required increases, so the high-side pressure of a transcritical cycle has a COP-maximizing value [31,32]. The range 78–165 bar was searched to find the optimum of this trade-off. A coarse 4-bar scan bracketed the maximum COP, and a golden-section search then refined the optimum value. This was done for every case, and the optimum pressure ranged from 93.8 to 143.5 bar. The pure CO_2 case at 48 °C sat just above Okasha and Müller's [30] 140 bar gas-cooler pressure validity limit, at 143.5 bar. The optimal pressure was re-determined independently for every case, including every ε in Section 2.8.

2.6 Exergy analysis

Exergy destruction in each component was obtained from the Gouy–Stodola relation [33,34], as in previous second-law analyses of transcritical CO_2 cycles [35,36]:

(4)

where s_{gen} is the entropy generated by the refrigerant stream together with any thermal reservoir it exchanges heat with, and $T_0 = T_{amb}$. Exergy destroyed is proportional to the ambient temperature multiplied by the entropy generated by the process. The exergy supplied as compressor work becomes useful cooling if it is not destroyed by the components or rejected with the heat leaving the gas cooler. All three parts sum back to the compressor work, and the balance closes to within numerical round-off in every case. The second-law efficiency is

(5)

with temperatures in kelvin. The exergy results reported in Section 3.5 are for the IHX cycle. Because T_0 varies with ambient temperature, absolute destructions at different ambient temperatures are referenced to different dead states; component shares are directly comparable.

2.7 Total equivalent warming impact

To find the TEWI of the blend and compare it with pure CO_2, both direct contributions to global warming (refrigerant leakage and end-of-life release) and indirect contributions from electricity consumption were added, following the established TEWI method [37–39]. The TEWI is given by

(6)

where the global warming potential of the blend is

(7)

and the annual electricity consumption is

(8)

The COP used is that of the IHX cycle. Parameter values are given in Table 2. The 100-year GWP values are taken from the IPCC Sixth Assessment Report for CO_2 [40] and from [41,42] for R-1270. The grid emission factor is the IEA value for Saudi Arabia [43]; the lower official factor of 0.568 kg CO_2 kWh^{-1} for 2021 [44] would reduce the indirect contribution proportionally.

2.8 IHX sensitivity analysis

The IHX effectiveness ε was varied from 0 to 0.9 in steps of 0.1. This was done for both the 40 °C and 48 °C cases, including both pure CO_2 and the 10% zeotropic blend. At every ε step, the high-side pressure was optimized again.

3. Results

3.1 Baseline COP

Plotted against R-1270 mass fraction, baseline COP falls with both increases in ambient temperature and increases in R-1270. At 40 °C, pure CO_2 has a COP of 1.53, while it has a COP of 1.15 at 48 °C. This is a 25% drop in COP, and all curves slope similarly (Fig. 3).

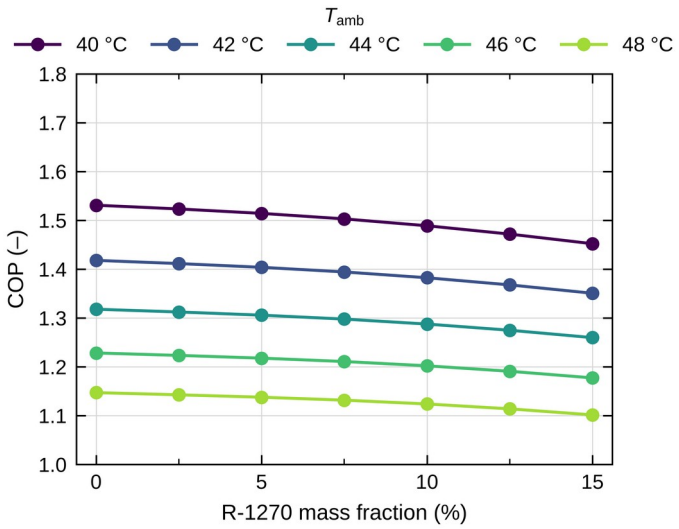


Fig. 3. Baseline (no-IHX) COP against R-1270 mass fraction at each ambient temperature.

3.2 Blend penalty

The change in COP relative to that of pure CO_2 is negative at all compositions and ambient temperatures. At 15% R-1270, it was −5.2% at 40 °C and −4.0% at 48 °C. The COP penalty grows as the fraction of R-1270 increases, but decreases as ambient temperature increases (Fig. 4).

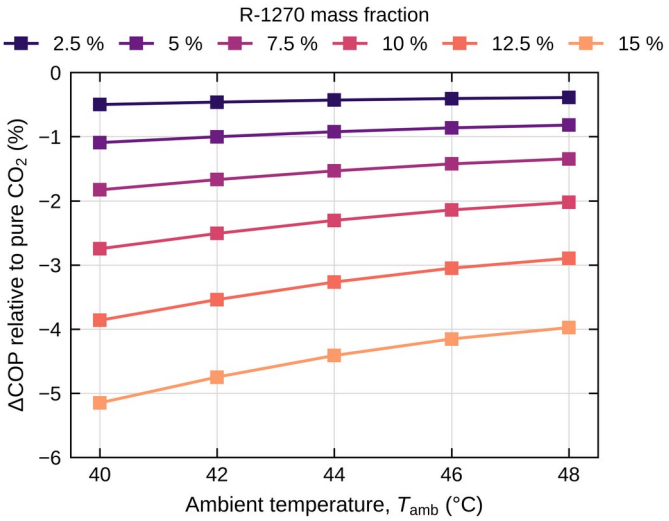


Fig. 4. Change in baseline COP relative to pure CO_2 against ambient temperature for each R-1270 mass fraction.

3.3 Optimal high-side pressure

The optimal high-side pressure increased as the ambient temperature increased, but decreased as the fraction of R-1270 in the blend increased. With internal heat exchange, the optimal pressure fell. The optimal pressure ranged from 98.1 to 143.5 bar without the IHX and from 93.8 to 130.6 bar with it (Fig. 5).

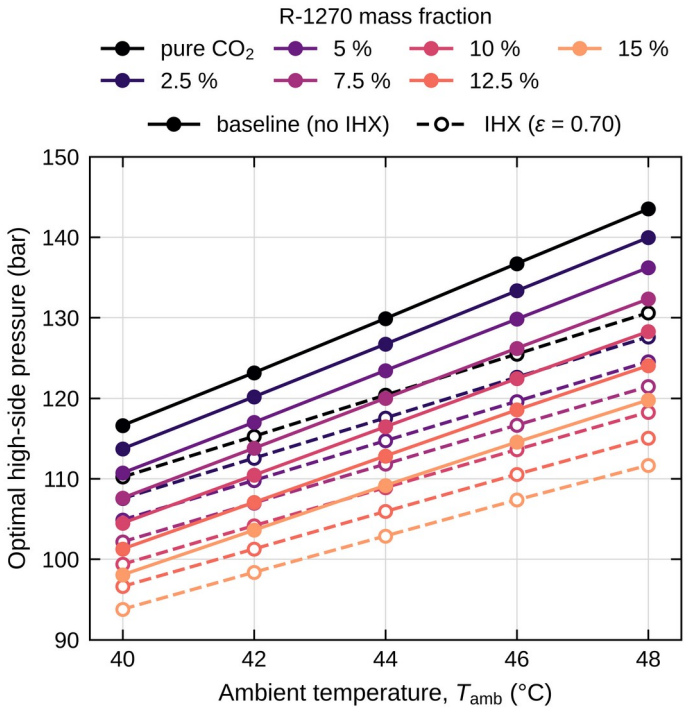


Fig. 5. COP-optimal high-side pressure against ambient temperature. Solid lines, filled markers: baseline cycle; dashed lines, open markers: with IHX (ε = 0.70).

3.4 Effect of the IHX

In all cases, the IHX raised the COP. For pure CO_2, the COP increased by 7.7% at 40 °C and by 13.0% at 48 °C. The COP gain increases with ambient temperature, and the blend penalty still lowers the COP with the IHX (Fig. 6).

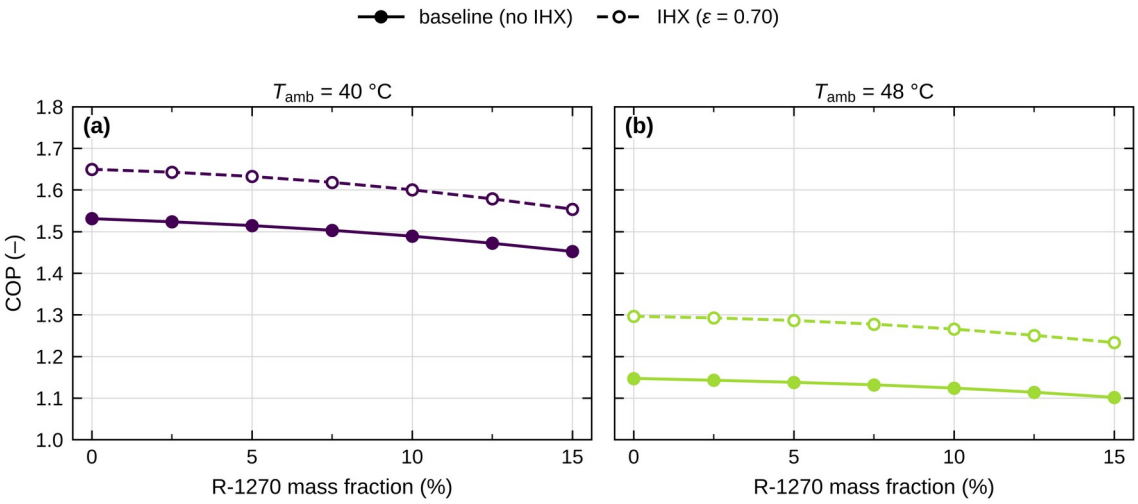


Fig. 6. COP with and without the IHX against R-1270 mass fraction at (a) 40 °C and (b) 48 °C ambient. Solid lines, filled markers: baseline; dashed lines, open markers: with IHX (ε = 0.70).

3.5 Exergy destruction

The compressor is the largest destroyer of exergy in the IHX cycle (39–42%), followed by the gas cooler (32–35%), the valve (19–20%), the IHX (4–5%), and lastly the evaporator (0–4%). The second-law efficiency η_{II} of the IHX cycle was 0.19–0.21 (Fig. 7).

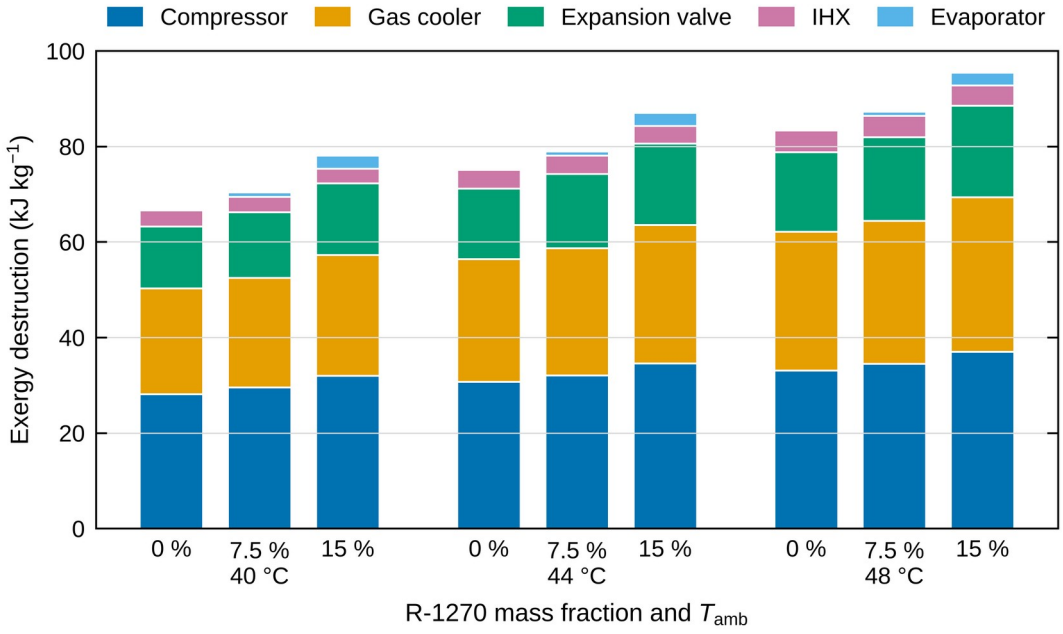


Fig. 7. Component exergy destruction in the IHX cycle at 40, 44 and 48 °C ambient for 0, 7.5 and 15% R-1270.

3.6 TEWI

Over the 15-year lifetime, the TEWI was between 38.0 and 50.8 t CO_2-eq. As the ambient temperature increased, the emissions also increased. Direct emissions were below 0.01% of total emissions (Fig. 8).

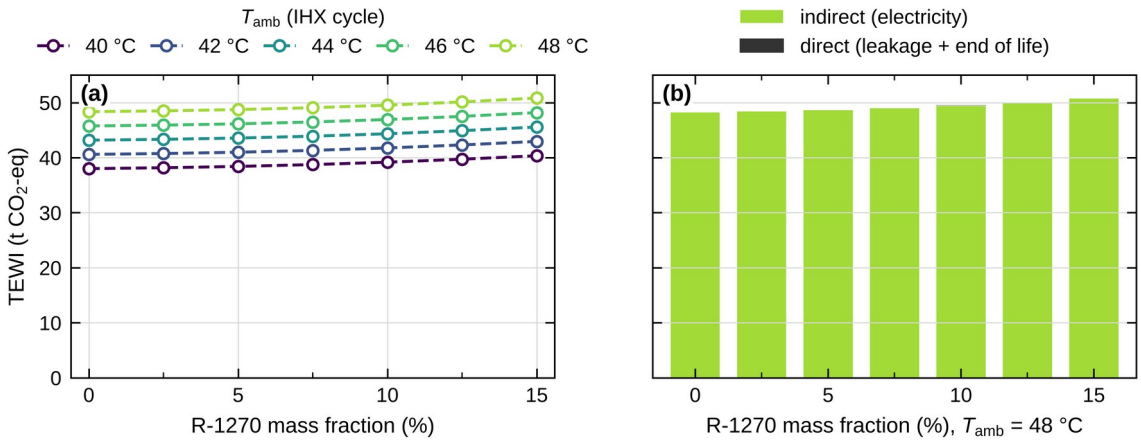


Fig. 8. (a) TEWI of the IHX cycle against R-1270 mass fraction at each ambient temperature; (b) direct and indirect contributions at 48 °C. The direct contribution (below 0.01%) is not visible at this scale.

3.7 IHX sensitivity

Across all ε values (0–0.9), the 10% R-1270 blend penalty lies between −2.0% and −3.1%, and it never crossed zero. The pure-CO_2 COP rose by 9.4% and 15.7% at 40 and 48 °C, respectively, as ε rose from 0 to 0.9 (Fig. 9).

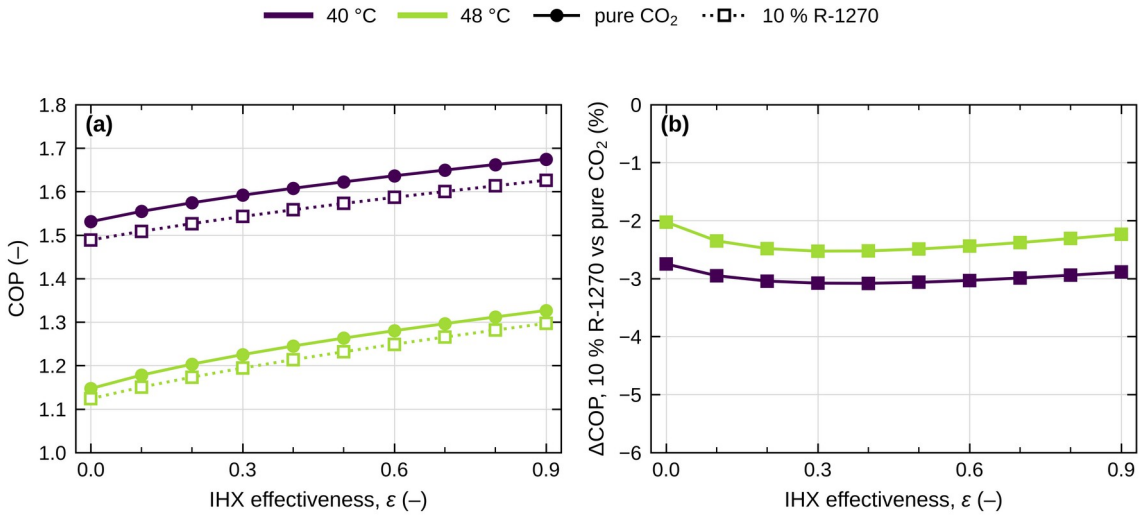


Fig. 9. (a) COP of pure CO_2 and the 10% blend against IHX effectiveness ε at 40 and 48 °C; (b) the corresponding blend penalty. The high-side pressure is re-optimized at every ε. Solid lines, filled circles: pure CO_2; dotted lines, open squares: 10% R-1270.

4. Discussion

4.1 Why the blend does not help

The zeotropic blend's critical temperature is very important when analysing the results: adding R-1270 raises the mixture's critical temperature compared with pure CO_2. The critical temperature was 31.0 °C for pure CO_2 and increased to 37.2 °C at 15% R-1270, an increase of 6.2 K. However, the gas cooler outlet is between 45 and 53 °C, and this requires a rise of at least 14 K for the outlet to drop below the critical point of the mixture. It follows that the thermodynamic cycle stays transcritical at every composition, and the benefit of condensation is never realized with R-1270. Volumetric capacity drops because the lower evaporator pressure means a lower vapour density; the evaporator pressure goes from 39.7 to 29.9 bar, and the glide reaches 6.4 K. Fig. 10 shows the mixture critical locus against the gas-cooler outlet band.

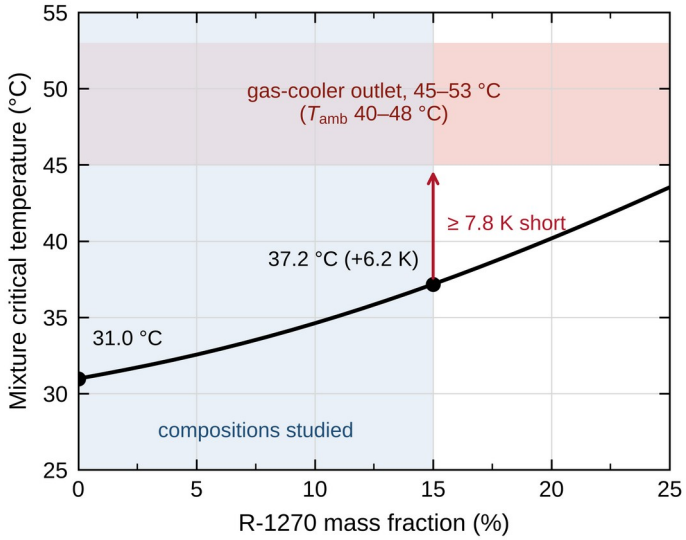


Fig. 10. Critical temperature of the CO_2/R-1270 mixture against R-1270 mass fraction (CoolProp 8.0.0 [24,29]). The shaded band is the gas-cooler outlet temperature for 40–48 °C ambient. At 15% R-1270 the critical temperature rises 6.2 K; at least 14 K would be required.

4.2 Why the penalty shrinks with ambient temperature

The absolute COP gap shrinks from 0.08 at 40 °C to 0.05 at 48 °C, a drop of about 40%, whereas the COP of pure CO_2 falls by 25%. The blend's optimal pressure is lower than that of pure CO_2 at both ends: 98.1 bar against 116.6 bar at 40 °C (−15.9%), and 119.8 bar against 143.5 bar at 48 °C (−16.5%). The gap widens slightly, from 18.6 bar to 23.7 bar. In the IHX cycle, the 15% blend requires more compressor work than pure CO_2: 102.2 against 88.7 kJ kg^{-1} at 40 °C (+15.2%), and 123.2 against 109.1 kJ kg^{-1} at 48 °C (+13.0%), so the extra work shrinks as the ambient temperature rises. The blend's refrigerating effect is also higher: 158.8 against 146.4 kJ kg^{-1} at 40 °C (+8.5%), and 151.9 against 141.4 kJ kg^{-1} at 48 °C (+7.5%). In all cases, the zeotropic blend

needs more extra work than it gains in cooling effect, and this is why the COP drops. However, the extra work falls by about 2.2 percentage points between 40 and 48 °C, while the extra cooling effect falls by only about 1.1. Therefore, the work penalty of the zeotropic blend shrinks faster than its cooling advantage. This is not caused by the pressure ratio, whose penalty for the blend grows slightly from 12.9% to 13.5%, nor by the compressor efficiency, which differs by the same 0.4% at both temperatures. Instead, because the dew point is fixed at 5 °C, the blend's evaporator pressure stays at 29.9 bar against 39.7 bar for pure CO_2 at every ambient temperature, so the blend pays a nearly constant extra work of 13.5–14.1 kJ kg^{-1} to compress from this lower suction pressure. As the total compressor work rises with ambient temperature, this nearly fixed extra work becomes a smaller fraction of the total.

4.3 Why the IHX gain grows with ambient temperature

At high ambient temperatures, there is a much larger gap between the gas cooler outlet temperature T_3 and the evaporator outlet temperature T_1. This increases the amount of heat that the internal heat exchanger can transfer. Consequently, the throttling loss that it helps offset grows with the ambient temperature.

4.4 Design implication

In harsh Gulf summer conditions, effort should be put into optimizing the internal heat exchanger and expansion-work recovery [35] rather than zeotropic blends. The split in exergy supports this, as the compressor and valve together destroy 60% of the exergy.

4.5 Flammability

R-1270 is ASHRAE safety class A3 [45]. Sánchez et al. [6] derived CO_2/R-1270 compositions that are theoretically non-flammable at low R-1270 fractions, but the flammability of the higher fractions studied here, up to 15%, has not been established, so they should be treated as potentially flammable. The refrigerant charge would then be limited by ISO 5149-1 [46] and IEC 60335-2-89 [47], which raises questions about the practical viability of installing a 15% blend.

4.6 Limitations and comparison with experiments

The limitations associated with the model include the absence of a departure function in the mixture model. The results were checked against simulations and not against experiments. The model runs at only one evaporating temperature. The discharge temperatures are an upper bound because of the adiabatic compressor model. The approach temperature is fixed and there are no pressure drops. The model cannot represent glide matching, which is how published blend studies obtain their gains [9,19].

Under the mean and bubble-point conventions for the evaporating temperature, the change in COP at 15% R-1270 and 40 °C becomes +3.1% and +11.8%, respectively. Under these conventions the blend's evaporator is warmer than that of pure CO_2: fixing the bubble point at 5 °C puts the dew point of the 15% blend at 11.4 °C. These conventions therefore compare a zeotropic blend cooling a space to 11 °C against pure CO_2 cooling it to 5 °C, and the blend is favoured because it does less work than its counterpart. When the dew point is fixed, the coldest useful outlet state and the compressor suction temperature are controlled across all compositions in the investigation.

Larrondo-Sancho et al. [23] reported +9.7% COP at 4% R-1270, while the present model gives −0.9% at that composition. Three differences may explain this. First, their heat-rejection temperatures (20–34 °C) lie close to the mixture critical temperature, whereas the gas-cooler outlet here (45–53 °C) lies 8–22 K above it at every composition. Second, they attribute most of the gain to improved compressor efficiency with the mixtures, and compressor behaviour is known to change with CO_2-based mixtures [21]; the present model applies the same η_{is}(PR) correlation to pure CO_2 and the blend, so it cannot reproduce this effect. Third, their heat exchangers and evaporator convention allow glide matching, which the fixed-approach, fixed-dew-point model excludes. The experimental results remain important because they come from a real transcritical rig with an IHX; testing the blend in such a rig at 40–48 °C ambient is the natural next step.

5. Conclusions

1. The blend penalty associated with R-1270 exists at every composition and ambient temperature, with a change in COP of −5.2% at 15% R-1270 and 40 °C.

2. The critical temperature rises 6.2 K while 14 K is required to bring the system below the critical point. Therefore, the cycle stays transcritical throughout the investigation.

3. As the ambient temperature increases, the blend penalty decreases from −5.2% at 40 °C to −4.0% at 48 °C. This was attributed to the blend's work penalty shrinking faster than its cooling advantage, because the extra work needed to compress from the blend's lower suction pressure stays nearly constant while the total compressor work rises with ambient temperature.

4. The internal heat exchanger proved helpful in recovering COP, recovering 7.7% to 13.0%, but never rescued the blend at any ε.

5. To make designs more efficient, the internal heat exchanger and the recovery of expansion work should remain a priority over zeotropic blending. The compressor and the valve together destroy 60% of the exergy.

Nomenclature

COP	coefficient of performance (–)
E_{annual}	annual electricity consumption (kWh yr^{-1})
GWP	global warming potential (–)
h	specific enthalpy (kJ kg^{-1})
I	specific exergy destruction (kJ kg^{-1})
L_{annual}	annual leakage rate (yr^{-1})
m	refrigerant charge (kg)
n	system lifetime (yr)
p	pressure (bar)
PR	compressor pressure ratio p_{high}/p_{evap} (–)
q	specific heat transfer (kJ kg^{-1})
Q_{ref}	reference cooling duty (kW)
s	specific entropy (kJ kg^{-1} K^{-1})
T	temperature (°C; K in Eqs. (4)–(5))
w	specific work (kJ kg^{-1})
x	R-1270 mass fraction (–)

Greek

α_{rec}	end-of-life recovery fraction (–)
β	grid emission factor (kg CO_2 kWh^{-1})
β_T, γ_T, β_V, γ_V	mixture reducing parameters (–)
ΔT_{app}	gas-cooler approach temperature (K)
ε	IHX temperature effectiveness (–)
η_{is}	compressor isentropic efficiency (–)
η_{II}	second-law efficiency (–)
τ	annual full-load operating hours (h yr^{-1})

Subscripts

0	dead state
1, 1b, 2, 2s, 3, 3b, 4	cycle state points (Fig. 1)
amb	ambient
comp	compressor
evap	evaporator
gc	gas cooler
gen	generated
high	high-pressure side
ihx	internal heat exchanger

Abbreviations

GWP	global warming potential
HEOS	Helmholtz-energy equation of state
IHX	internal heat exchanger
ODP	ozone depletion potential
TEWI	total equivalent warming impact
VCC	volumetric cooling capacity

Declaration of competing interest

The author declares no known competing financial interests or personal relationships that could have appeared to influence the work reported in this paper.

CRediT authorship contribution statement

Abdulaziz Alsahali: Conceptualization, Methodology, Software, Validation, Formal analysis, Investigation, Data curation, Writing – original draft, Writing – review & editing, Visualization.

Data availability

The cycle model (Python, CoolProp 8.0.0), all computed datasets and the figure-generation scripts are available from the author on request.

Funding

This research did not receive any specific grant from funding agencies in the public, commercial, or not-for-profit sectors.

Declaration of generative AI and AI-assisted technologies in the writing process

During the preparation of this work the author used Claude (Anthropic) to check spelling, grammar and notation, to convert first-person sentences to impersonal voice, to summarise the literature and draft parts of the Introduction and Discussion (Sections 1, 4.5 and 4.6), to typeset equations and tables, to generate figures from the author's computed data, to draw the process scheme (Fig. 1), and to compile and verify the reference list. The author reviewed and edited all output and takes full responsibility for the content of the publication.

References

[1] G. Lorentzen, Revival of carbon dioxide as a refrigerant, Int. J. Refrig. 17 (5) (1994) 292–301. https://doi.org/10.1016/0140-7007(94)90059-0

[2] M.-H. Kim, J. Pettersen, C.W. Bullard, Fundamental process and system design issues in CO2 vapor compression systems, Prog. Energy Combust. Sci. 30 (2) (2004) 119–174. https://doi.org/10.1016/j.pecs.2003.09.002

[3] K.M. Tsamos, Y.T. Ge, I. Santosa, S.A. Tassou, G. Bianchi, Z. Mylona, Energy analysis of alternative CO2 refrigeration system configurations for retail food applications in moderate and warm climates, Energy Convers. Manag. 150 (2017) 822–829. https://doi.org/10.1016/j.enconman.2017.03.020

[4] N. Purohit, V. Sharma, S. Sawalha, B. Fricke, R. Llopis, M.S. Dasgupta, Integrated supermarket refrigeration for very high ambient temperature, Energy 165 (Part A) (2018) 572–590. https://doi.org/10.1016/j.energy.2018.09.097

[5] L. Chai, S.A. Tassou, K.M. Tsamos, Effects of rising ambient temperature on the performance of transcritical CO2 refrigeration systems, in: Proc. 1st IIR International Conference on Refrigeration Adapting to Rising Temperatures, 2024, Paper 1132. https://doi.org/10.18462/iir.adaptation.2024.1132

[6] D. Sánchez, F. Vidan-Falomir, L. Nebot-Andrés, R. Llopis, R. Cabello, Alternative blends of CO2 for transcritical refrigeration systems. Experimental approach and energy analysis, Energy Convers. Manag. 279 (2023) 116690. https://doi.org/10.1016/j.enconman.2023.116690

[7] D. Sánchez, R. Larrondo, F. Vidan-Falomir, R. Cabello, Experimental evaluation of the CO2-based mixtures CO2/R32, CO2/R1234yf and CO2/R1270 in a transcritical refrigerating plant considering the effect of the internal heat exchanger (IHX), Appl. Therm. Eng. 236 (2024) 121473. https://doi.org/10.1016/j.applthermaleng.2023.121473

[8] B. Dai, S. Liu, H. Li, Z. Sun, M. Song, Q. Yang, Y. Ma, Energetic performance of transcritical CO2 refrigeration cycles with mechanical subcooling using zeotropic mixture as refrigerant, Energy 150 (2018) 205–221. https://doi.org/10.1016/j.energy.2018.02.111

[9] J.H. Kim, J.M. Cho, M.S. Kim, Cooling performance of several CO2/propane mixtures and glide matching with secondary heat transfer fluid, Int. J. Refrig. 31 (5) (2008) 800–806. https://doi.org/10.1016/j.ijrefrig.2007.11.009

[10] C. Aprea, A. Maiorino, An experimental evaluation of the transcritical CO2 refrigerator performances using an internal heat exchanger, Int. J. Refrig. 31 (6) (2008) 1006–1011. https://doi.org/10.1016/j.ijrefrig.2007.12.016

[11] S. Elbel, P. Hrnjak, Experimental validation of a prototype ejector designed to reduce throttling losses encountered in transcritical R744 system operation, Int. J. Refrig. 31 (3) (2008) 411–422. https://doi.org/10.1016/j.ijrefrig.2007.07.013

[12] P. Gullo, B. Elmegaard, G. Cortella, Energy and environmental performance assessment of R744 booster supermarket refrigeration systems operating in warm climates, Int. J. Refrig. 64 (2016) 61–79. https://doi.org/10.1016/j.ijrefrig.2015.12.016

[13] J. Sarkar, N. Agrawal, Performance optimization of transcritical CO2 cycle with parallel compression economization, Int. J. Therm. Sci. 49 (5) (2010) 838–843. https://doi.org/10.1016/j.ijthermalsci.2009.12.001

[14] E. Torrella, D. Sánchez, R. Llopis, R. Cabello, Energetic evaluation of an internal heat exchanger in a CO2 transcritical refrigeration plant using experimental data, Int. J. Refrig. 34 (1) (2011) 40–49. https://doi.org/10.1016/j.ijrefrig.2010.07.006

[15] R. Cabello, D. Sánchez, R. Llopis, E. Torrella, Experimental evaluation of the energy efficiency of a CO2 refrigerating plant working in transcritical conditions, Appl. Therm. Eng. 28 (13) (2008) 1596–1604. https://doi.org/10.1016/j.applthermaleng.2007.10.026

[16] N. Purohit, D.K. Gupta, M.S. Dasgupta, Experimental investigations of CO2 trans-critical refrigeration system with and without internal heat exchanger for warm climate, in: Proc. 13th IIR Gustav Lorentzen Conference on Natural Refrigerants (GL2018), Valencia, Spain, 18–20 June 2018, Paper 1337. https://doi.org/10.18462/iir.gl.2018.1337

[17] B. Dai, C. Dang, M. Li, et al., Thermodynamic performance assessment of carbon dioxide blends with low-global warming potential (GWP) working fluids for a heat pump water heater, Int. J. Refrig. 56 (2015) 1–14.

[18] B. Yu, D. Wang, C. Liu, F. Jiang, J. Shi, J. Chen, Performance improvements evaluation of an automobile air conditioning system using CO2-propane mixture as a refrigerant, Int. J. Refrig. 88 (2018) 172–181. https://doi.org/10.1016/j.ijrefrig.2017.12.016

[19] S.C. Yelishala, K. Kannaiyan, R. Sadr, Z. Wang, Y.A. Levendis, H. Metghalchi, Performance maximization by temperature glide matching in energy exchangers of cooling systems operating with natural hydrocarbon/CO2 refrigerants, Int. J. Refrig. 119 (2020) 294–304. https://doi.org/10.1016/j.ijrefrig.2020.08.006

[20] S.C. Yelishala, K. Kannaiyan, Z. Wang, H. Metghalchi, Y.A. Levendis, R. Sadr, Thermodynamic study on blends of hydrocarbons and carbon dioxide as zeotropic refrigerants, J. Energy Resour. Technol. 142 (8) (2020) 082304. https://doi.org/10.1115/1.4045930

[21] D. Sánchez, R. Larrondo-Sancho, F. Vidan-Falomir, R. Cabello, Empirical modelling of a semihermetic reciprocating compressor for different CO2-based mixtures, Appl. Therm. Eng. 250 (2024) 123536. https://doi.org/10.1016/j.applthermaleng.2024.123536

[22] F. Vidan-Falomir, R. Larrondo-Sancho, D. Sánchez, R. Cabello, Experimental comparison of CO2 and alternative CO2/R1270 mixtures in a transcritical refrigerating plant. Energy evaluation in an MT application, in: Proc. 16th IIR-Gustav Lorentzen Conference on Natural Refrigerants (GL2024), College Park, MD, USA, 11–14 August 2024, Paper 1107. https://doi.org/10.18462/iir.gl2024.1107

[23] R. Larrondo-Sancho, D. Sánchez, R. Cabello, Experimental evaluation of natural CO2-based mixtures with hydrocarbons R290 and R1270 in a transcritical refrigeration plant, Int. J. Refrig. 178 (2025) 215–226. https://doi.org/10.1016/j.ijrefrig.2025.06.034

[24] I.H. Bell, J. Wronski, S. Quoilin, V. Lemort, Pure and pseudo-pure fluid thermophysical property evaluation and the open-source thermophysical property library CoolProp, Ind. Eng. Chem. Res. 53 (6) (2014) 2498–2508. https://doi.org/10.1021/ie4033999

[25] R. Span, W. Wagner, A new equation of state for carbon dioxide covering the fluid region from the triple-point temperature to 1100 K at pressures up to 800 MPa, J. Phys. Chem. Ref. Data 25 (6) (1996) 1509–1596. https://doi.org/10.1063/1.555991

[26] E.W. Lemmon, U. Overhoff, M.O. McLinden, W. Wagner, A reference equation of state for the thermodynamic properties of propene for temperatures from the melting line to 575 K and pressures up to 1000 MPa, unpublished equation of state (2010/2013), implemented in NIST REFPROP and CoolProp (fluid key "Lemmon-PROPYLENE-2013").

[27] U. Overhoff, Entwicklung einer neuen Zustandsgleichung für das fluide Zustandsgebiet von Propen für Temperaturen von der Schmelzlinie bis 575 K bei Drücken bis 1000 MPa sowie von Software zur Berechnung thermodynamischer Zustandsgrößen fluider Stoffe (Development of a new equation of state for the fluid region of propene …), Doctoral thesis, Ruhr-Universität Bochum, Germany, 2006. urn:nbn:de:hbz:294-17381. https://hss-opus.ub.rub.de/opus4/frontdoor/index/index/docId/870

[28] O. Kunz, W. Wagner, The GERG-2008 wide-range equation of state for natural gases and other mixtures: An expansion of GERG-2004, J. Chem. Eng. Data 57 (11) (2012) 3032–3091. https://doi.org/10.1021/je300655b

[29] I.H. Bell, E.W. Lemmon, Automatic fitting of binary interaction parameters for multi-fluid Helmholtz-energy-explicit mixture models, J. Chem. Eng. Data 61 (11) (2016) 3752–3760. https://doi.org/10.1021/acs.jced.6b00257

[30] A. Okasha, N. Müller, Simulation and performance correlation for transcritical CO2 heat pump cycle, in: Proc. 17th International Refrigeration and Air Conditioning Conference at Purdue, West Lafayette, IN, USA, 9–12 July 2018, Paper 2056. https://docs.lib.purdue.edu/iracc/2056

[31] S.M. Liao, T.S. Zhao, A. Jakobsen, A correlation of optimal heat rejection pressures in transcritical carbon dioxide cycles, Appl. Therm. Eng. 20 (9) (2000) 831–841. https://doi.org/10.1016/S1359-4311(99)00070-8

[32] J. Sarkar, S. Bhattacharyya, M. Ram Gopal, Optimization of a transcritical CO2 heat pump cycle for simultaneous cooling and heating applications, Int. J. Refrig. 27 (8) (2004) 830–838. https://doi.org/10.1016/j.ijrefrig.2004.03.006

[33] A. Bejan, Advanced Engineering Thermodynamics, 4th ed., John Wiley & Sons, Hoboken, NJ, 2016. https://doi.org/10.1002/9781119245964

[34] T.J. Kotas, The Exergy Method of Thermal Plant Analysis, Butterworths, London, 1985 (reprinted Krieger, Malabar, FL, 1995). ISBN 978-0-408-01350-5.

[35] J.L. Yang, Y.T. Ma, M.X. Li, H.Q. Guan, Exergy analysis of transcritical carbon dioxide refrigeration cycle with an expander, Energy 30 (7) (2005) 1162–1175. https://doi.org/10.1016/j.energy.2004.08.007

[36] A.E. Özgür, H.C. Bayrakçi, Second law analysis of two-stage compression transcritical CO2 heat pump cycle, Int. J. Energy Res. 32 (5) (2008) 1202–1209. https://doi.org/10.1002/er.1415

[37] AIRAH, Methods of Calculating Total Equivalent Warming Impact (TEWI) 2012 — Best Practice Guidelines, Australian Institute of Refrigeration, Air Conditioning and Heating, Melbourne, 2012.

[38] P. Makhnatch, R. Khodabandeh, The role of environmental metrics (GWP, TEWI, LCCP) in the selection of low GWP refrigerant, Energy Procedia 61 (2014) 2460–2463. https://doi.org/10.1016/j.egypro.2014.12.023

[39] A. Mota-Babiloni, J.R. Barbosa Jr., P. Makhnatch, J.A. Lozano, Assessment of the utilization of equivalent warming impact metrics in refrigeration, air conditioning and heat pump systems, Renew. Sustain. Energy Rev. 129 (2020) 109929. https://doi.org/10.1016/j.rser.2020.109929

[40] P. Forster, T. Storelvmo, K. Armour, W. Collins, J.-L. Dufresne, D. Frame, D.J. Lunt, T. Mauritsen, M.D. Palmer, M. Watanabe, M. Wild, H. Zhang, The Earth's energy budget, climate feedbacks, and climate sensitivity, in: V. Masson-Delmotte et al. (Eds.), Climate Change 2021: The Physical Science Basis. Contribution of Working Group I to the Sixth Assessment Report of the Intergovernmental Panel on Climate Change, Cambridge University Press, Cambridge, UK and New York, NY, 2021, pp. 923–1054. https://doi.org/10.1017/9781009157896.009

[41] Ø. Hodnebrog, B. Aamaas, J.S. Fuglestvedt, G. Marston, G. Myhre, C.J. Nielsen, M. Sandstad, K.P. Shine, T.J. Wallington, Updated global warming potentials and radiative efficiencies of halocarbons and other weak atmospheric absorbers, Rev. Geophys. 58 (3) (2020) e2019RG000691. https://doi.org/10.1029/2019RG000691

[42] D. Colbourne, A. Vonsild, Global warming potential of hydrocarbon refrigerants, in: Proc. 13th IIR Gustav Lorentzen Conference on Natural Refrigerants (GL2018), Valencia, Spain, 18–20 June 2018, Paper 1404. https://doi.org/10.18462/iir.gl.2018.1404

[43] IEA, Emissions Factors 2025 (annual GHG emission factors for electricity and heat generation, 1990–2023, provisional 2024), International Energy Agency, Paris, 2025. https://www.iea.org/data-and-statistics/data-product/emissions-factors-2025

[44] Designated National Authority (DNA) of the Kingdom of Saudi Arabia, Official grid emission factor for CDM projects, 2021: 0.568 tCO2/MWh (0.568 kg CO2/kWh), as cited in: KFUPM, Greenhouse Gas Emissions Inventory, King Fahd University of Petroleum & Minerals, Dhahran, 2022. https://sustainability.kfupm.edu.sa/documents/53/Greenhouse_Gas_Emissions_Inventory.pdf

[45] ANSI/ASHRAE Standard 34-2022, Designation and Safety Classification of Refrigerants, ASHRAE, Peachtree Corners, GA, 2022.

[46] ISO 5149-1:2014, Refrigerating systems and heat pumps — Safety and environmental requirements — Part 1: Definitions, classification and selection criteria, International Organization for Standardization, Geneva, 2014 (Amd 1:2015).

[47] IEC 60335-2-89:2019, Household and similar electrical appliances — Safety — Part 2-89: Particular requirements for commercial refrigerating appliances and ice-makers with an incorporated or remote refrigerant unit or motor-compressor, 3rd ed., International Electrotechnical Commission, Geneva, 2019.

Tables

Table 1. Operating conditions and model parameters.

Parameter	**Symbol**	**Value**	**Justification**
Evaporating temperature (dew point)	T_{evap}	5 °C	Representative of space-cooling duty; dew point fixed so the evaporator outlet state is identical for every composition
Gas-cooler approach temperature	ΔT_{app}	5 K	Finite gas-cooler area; air-cooled gas coolers operate slightly above ambient
Gas-cooler outlet temperature	T_3	T_{amb} + 5 K	Follows from the approach temperature
Compressor isentropic efficiency	η_{is}	0.59–0.60	Pressure-ratio correlation of Okasha and Müller [30], Section 2.4
Baseline IHX effectiveness	ε	0.70	Mid-range value representative of the 0–0.9 sweep in Section 2.8
IHX effectiveness sweep	ε	0–0.9, step 0.1	Sensitivity analysis, Section 2.8
Dead-state temperature	T_0	T_{amb} (40–48 °C)	Reference environment is the ambient air; varies by case
Dead-state pressure	p_0	1.013 bar	Atmospheric
High-side pressure search window	p_{high}	78–165 bar	Brackets all optima (93.8–143.5 bar, Section 2.5)
Ambient temperatures	T_{amb}	40, 42, 44, 46, 48 °C	Daytime Gulf summer conditions, when air-conditioning demand is at its peak [4,5]
R-1270 mass fractions	x	0, 2.5, 5, 7.5, 10, 12.5, 15%	Conventional zeotropic fraction range over which the ecological benefit of CO_2 is retained

Table 2. TEWI parameters.

Symbol	**Value**	**Description**	**Source**
m	2.0 kg	Refrigerant charge	assumed
L_{annual}	0.02 yr^{-1}	Annual leakage rate	[37]
n	15 yr	System lifetime	[37]
α_{rec}	0.70	End-of-life recovery fraction	[37]
GWP_{CO2}	1	100-yr GWP of CO_2	[40]
$GWP_{R\text{-}1270}$	3.3	100-yr GWP of R-1270	[41,42]
Q_{ref}	3.5 kW	Reference cooling duty	assumed

τ	2000 h yr^{-1}	Annual full-load operating hours	assumed
β	0.597 kg CO_2 kWh^{-1}	Saudi grid emission factor (2023 data)	[43]

Table 3. Published CO_2/R-1270 blend studies compared with the present study.

Study	**Blend (mass %)**	**Heat rejection**	**Configuration**	**Method**	**Reported change vs pure CO_2**
Sánchez et al. [6]	CO_2/R-1270, CO_2/R-32	25 and 30 °C ambient	Vertical display cooler	Experiment	Energy use −17.2% (25 °C), −12.2% (30 °C)
Vidan-Falomir et al. [22]	CO_2/R-1270 97/3, 94/6, 91/9	20–34 °C	Transcritical plant, MT	Experiment	COP up to +12.2%
Larrondo-Sancho et al. [23]	CO_2/R-1270 96/4, 94/6; CO_2/R-290 96/4, 94/6	20, 27, 34 °C	Single stage with IHX	Experiment	COP up to +9.7% (4% R-1270)
Present study	CO_2/R-1270, 0–15% R-1270	45–53 °C (gas-cooler outlet; 40–48 °C ambient)	Single stage, with and without IHX	Model	COP −0.4% to −5.2% (baseline)